Available online at www.sciencedirect.com

ScienceDirect

Mendeleev Commun., 2019, **29**, 405–407

Mendeleev Communications

Disorder–order phase transition in nanocrystalline titanium monoxide with two-sublattice ordering of structural vacancies

Maxim G. Kostenko[a] and Albina A. Valeeva*[a,b]

[a] *Institute of Solid State Chemistry, Ural Branch of the Russian Academy of Sciences, 620990 Ekaterinburg, Russian Federation. Fax: +7 343 374 4495; e-mail: valeeva@ihim.uran.ru*

[b] *NANOTECH Centre, Ural Federal University, 620002 Ekaterinburg, Russian Federation*

DOI: 10.1016/j.mencom.2019.07.016

Atomic-vacancy ordering was achieved *via* prolonged annealing of nanocrystalline nonstoichiometric titanium monoxide TiO_y possessing the average crystal size of ~30 ± 10 nm *in vacuo* in the temperature range of 300–1200 K. The XRD and HRTEM data revealed the ordering based on the orthorhombic superstructures of M_2X_3 and M_3X_2 types (space group *Immm*), which are derived from the *B*1 structure of disordered cubic phase of γ-TiO.

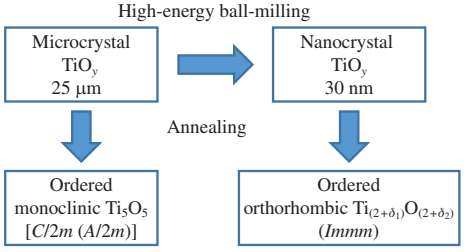

Titanium monoxide TiO_y contains an anomalously high concentration of structural vacancies (up to 30 at%), which causes a strong non-stoichiometry and is a prerequisite for the atomic-vacancy ordering. The exact amount of ordered phases in TiO_y is not yet known. The superstructure of stoichiometric composition M_5X_5 with monoclinic symmetry discovered by Hilti[1,2] and Watanabe *et al.*[3–5] and studied in detail,[6–11] as well as the cubic superstructure of the same type M_5X_5 proposed by Gusev[12–14] are the only examples of two-sublattice vacancy ordering confirmed experimentally. In the case of composition $TiO_{1.0}$, orthorhombic and tetragonal superstructures are theoretically possible.[15] A hybrid model was also considered,[16–20] where a part of defects was ordered by monoclinic type and the other part by cubic type M_5X_5. A tetragonal M_4X_5 superstructure[21] with an ordering in the oxygen sublattice is characteristic of the ordered phase possessing a composition close to $TiO_{1.25}$.

The orthorhombic phase with supposed M_2X_3-type superstructure in the range of compositions $TiO_{1.00}$–$TiO_{1.50}$ is also known.[1] One more orthorhombic phase belonging to *Immm* or *I*222 space groups was observed[4,5] in the range of $TiO_{0.7}$–$TiO_{0.9}$ that is closer to the model M_3X_2 of nominal composition $MX_{0.67}$. The theoretical analysis[22] revealed that the both superstructures are inverse to each other and should belong to *Immm* space group.

Herein we report on the simultaneous vacancy ordering of M_2X_3 type in metal sublattice and of M_3X_2 type in nonmetal sublattice observed experimentally in nanocrystalline nonstoichiometric TiO_y. The new ordered phase can be described by the superstructure of a two-sublattice ordering of the M_2X_2 type (space group *Immm*). To denote the new superstructure, the formula $M_{(2+\delta_1)}X_{(2+\delta_2)}$ is proposed, where parameters δ_1 and δ_2 reflect the presence of a fraction of atoms in the vacancy sublattices.

The initial microcrystals of nonstoichiometric TiO_y with an average size of about 25 μm were synthesized *via* the solid-phase sintering from a mixture of titanium and titanium dioxide powders *in vacuo* (10^{-3} Pa) at 1770 K. To achieve either disordered or ordered state, additional heat treatments at different regimes were performed.[7] Nanocrystalline powder with a mean nanoparticle size of ~30 ± 10 nm was produced by high-energy milling in a Retsch PM 200 planetary-type ball mill.[23] Along with the reduction of particle sizes, microdeformations of crystal lattice appeared during the milling. These deformations did not exceed 0.3% for the ordered samples and 0.85% for disordered ones. It is known that the milling leads to disordering and a reduction in the degree of long-range order parameter.[24] The structure and microstructure of microcrystalline and nanocrystalline nonstoichiometric TiO_y powders were examined using XRD, SEM and HRTEM methods.

According to the XRD data (Figure 1), the TiO_y nanopowder consisted of only one cubic TiO_y (space group $Fm\bar{3}m$) phase. Prolonged annealing of TiO_y nanopowder in the temperature range from 300 to 1200 K *in vacuo* (~10^{-3} Pa) led to the structural changes. Three phases have been identified; two of them, Ti_3O_5 (space group *I*2*c*) and TiO_2 (anatase), were not related to the atomic-vacancy ordering, whereas the third phase (space group

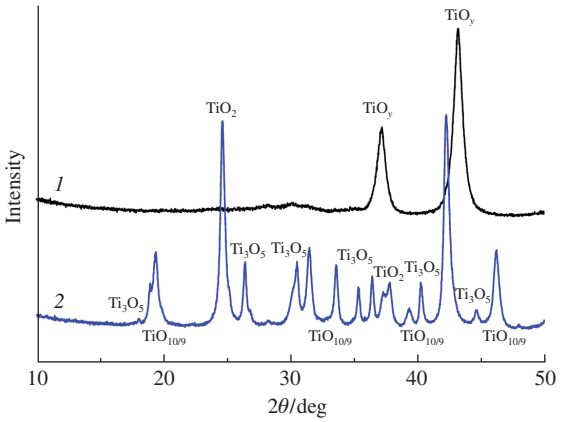

Figure 1 XRD patterns of titanium monoxide powders: (*1*) nanocrystalline sample after high-energy ball-milling, containing cubic TiO_y phase and (*2*) nanocrystalline sample annealed at 1200 K and quenched from 1200 K to room temperature (phases: Ti_3O_5, $TiO_{10/9}$, and TiO_2).

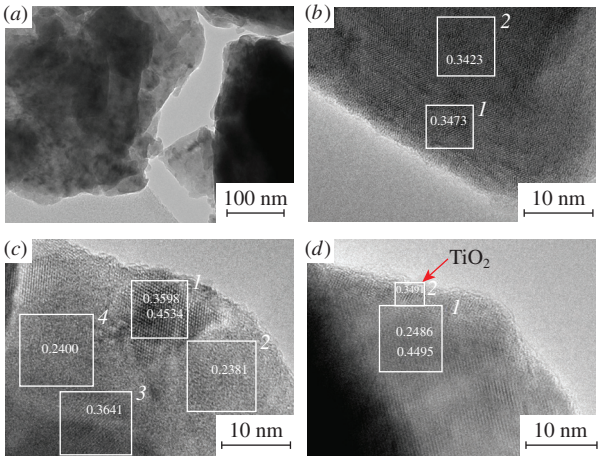

Figure 2 HRTEM images: (*a*) morphology of nanocrystalline titanium monoxide after high-energy ball-milling, (*b*) microstructure of particles with interplanar spacing (squares *1* and *2*) corresponding to the structure of Ti_3O_5, (*c*) microstructure of $TiO_{10/9}$ phase with good crystallinity, containing poorly crystallized particles with interplanar spacing (squares *1*–*4*) corresponding to the structure of $TiO_{10/9}$, and (*d*) particle of anatase (TiO_2) indicated by a red arrow in the matrix of $TiO_{10/9}$ phase.

Immm) of the $TiO_{10/9}$ composition contained about 25 and 16.7 at% of ordered vacancies in the metal and nonmetal sublattices, respectively. The $TiO_{10/9}$ phase was prepared according to the known procedure.[22]

Figure 2 shows the HRTEM images of TiO_y nanopowder. According to these data, ball-milled TiO_y nanopowder [see Figure 2(*a*)] consists of lamellar particles agglomerates, the plate-like particles widely ranging in the size (from 10 to 500 nm), and the uniformity of contrast in the particle is observed. There are regions with a lattice strain and mosaicity, which look as distortions of extinction lines on the particle surface. The particles belonging to the Ti_3O_5 phase [see Figure 2(*b*)] are flat-shaped crystallites sized from 50 nm and larger. The $TiO_{10/9}$ phase is presented by particles sized from 10 to 200 nm [see Figure 2(*c*)]. There are regions with both good crystallinity and distortions of crystalline order with interplanar spacing corresponding to the structure of $TiO_{10/9}$. A red arrow in Figure 2(*d*) indicates the location of the anatase (TiO_2) particles.

The ordered $TiO_{10/9}$ structure (*Immm*) is derived from *B*1 structure of the initial disordered monoxide. The ordering of vacancies occurs *via* their distribution in specific atomic planes alternating in certain sequence, *viz.*, the vacancy sites are in the each third plane $(001)_{ort}$ of orthorhombic structure [plane $(110)_{B1}$ of the basic *B*1 structure] separated from each other by two defect-free planes. Each defective plane contains approximately 75 at% of vacancies in the metal sublattice and 50 at% of vacancies in the nonmetal sublattice. The redistribution of vacancies upon ordering leads to the orthorhombic distortions of basic structure. The orthorhombic unit cell parameters are $a = 298.60$, $b = 915.42$ and $c = 392.60$ pm, and $\alpha = \beta = \gamma = 90°$.

If all the sites of defective planes of the ordered phase were vacant, it would have a stoichiometric composition $y = 1.00$ and would be described by superstructure M_2X_2, which had never been observed experimentally. This ordering model can be represented as a superposition of the orthorhombic superstructures of types M_2X_3 and M_3X_2 mentioned above. The latter was recently found in nonstoichiometric vanadium carbide containing vacancies only in the nonmetallic sublattice of the *B*1 structure.[25] Figure 3 shows the position of unit cells of M_2X_3 and M_3X_2 superstructures in the basic structure. Taking into account the real composition of ordered phase, one should use formula $Ti_{(2+\delta_1)}O_{(2+\delta_2)}$. In that case, $\delta_1 = 0.25$ and $\delta_2 = 0.50$.

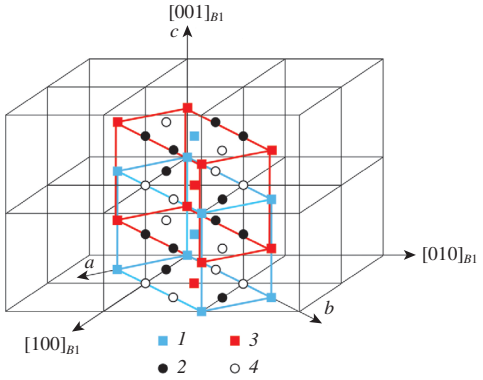

Figure 3 Position of combined vacancy sublattices of M_2X_3 (blue lines) and M_3X_2 (red lines) superstructures in the basic *B*1 crystal structure: (*1*) vacancy in the metal sublattice, (*2*) atom in the metal sublattice, (*3*) vacancy in the nonmetal sublattice and (*4*) atom in the nonmetal sublattice. The undistorted unit cell of the ordered orthorhombic phase is chosen to coincide with the unit cell of M_2X_3 superstructure. The unit cell boundaries of *B*1 structure, its directions, and the crystallographic axes of the superstructures are also shown.

Figure 4 shows the distribution of the O 2*p* and Ti 3*d* density of electronic states calculated for the disordered cubic phase $TiO_{10/9}$, ordered phase $Ti_{(2+\delta_1)}O_{(2+\delta_2)}$, and energetically favorable[33] ordered phase Ti_5O_5 using DFT[26–29] and supercell method.[30] The statical displacements of atoms were taken into account by relaxation of the atomic positions.

The width of the *p*–*d* gap region between the O 2*p* and Ti 3*d* states in the orthorhombic ordered phase is greater than that in the disordered cubic phase. Upon the formation of $Ti_{(2+\delta_1)}O_{(2+\delta_2)}$, the shape and width of the O 2*p* band mainly change, while the band of Ti 3*d* states remains unchanged. In particular, there is no deepening of the dip in the distribution of the density of Ti 3*d*

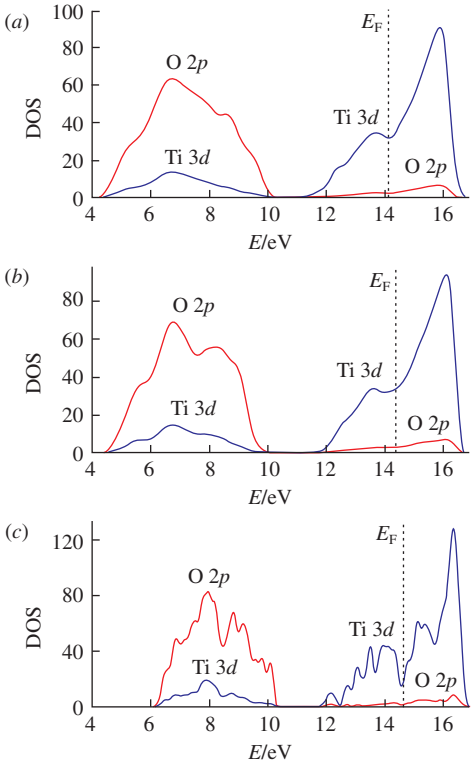

Figure 4 The calculated energy distribution of the density of electronic states for (*a*) disordered cubic $TiO_{10/9}$, (*b*) ordered $Ti_{(2+\delta_1)}O_{(2+\delta_2)}$ at $\delta_1 = 0.25$ and $\delta_2 = 0.50$, and (*c*) energetically favorable ordered Ti_5O_5 (see ref. 33). The density values are normalized to the cell containing 96 sites of the basic *B*1 structure.

states at the Fermi level, which is characteristic of energetically favorable superstructures.[31–34]

The cohesive energy E_{coh} was calculated as an energy characteristic of the phases according to the formula: $E_{coh} = (E - N_{Ti}E_{Ti} - N_O E_O)/N$, where E is the total energy of investigated phase per one superstructure; N_{Ti} and N_O are the numbers of titanium and oxygen atoms in a supercell, respectively; E_{Ti} and E_O are the total energies of titanium and oxygen atoms, respectively, taking into account the spin polarization effect, and N is the number of $TiO_{10/9}$ structural units in a supercell (equal to the number of titanium atoms). Thus, E_{coh} was -14.35 ± 0.04 eV for the disordered state and -14.34 ± 0.04 eV for the ordered phase. Therefore, the ordering in $TiO_{10/9}$ of $M_{(2+\delta_1)}X_{(2+\delta_2)}$ type does not provide any energy benefit as compared to the statistical distribution of defects.

To date, this is the only one known case, where an experimentally confirmed superstructure is energetically disadvantageous in comparison with a disordered phase. One among possible explanations may be that the ordering model constructed from X-ray diffraction data does not take into account the fine effects of local atomic-vacancy ordering, which lower the energy of defect structure.[34,35] Accounting for a short-range order within only the defective planes at vacancy concentration of 50 and 75 at% would inevitably lead to the appearance of a long-range order (*i.e.*, two-dimensional ordering). However, in this case, specific reflections on the XRD spectra will possess an extremely low intensity, making difficult their experimental identification. It seems that the influence of dimensional and surface effects on ordering is more probable. This was partially confirmed by the data[25] on the formation of M_3X_2 superstructure beginning at the grain boundaries and surface of the disordered phase with the $B1$ structure.

The ordering of microcrystalline nonstoichiometric TiO_y results in the formation of α-TiO phase with monoclinic superstructure M_5X_5 [space group $C2m$ ($A2m$)] in contrast to nanocrystalline TiO_y. In the case of nanocrystalline nonstoichiometric TiO_y with the relative oxygen content $y > 1$, a simultaneous ordering of structural vacancies in the metal and nonmetal sublattices was observed. The ordering of nanocrystalline TiO_y occurs in the orthorhombic superstructures of M_2X_3 and M_3X_2 types (space group *Immm*). The vacancy sublattices of $Ti_{(2+\delta_1)}O_{(2+\delta_2)}$ phase are partly disordered due to deviations from the stoichiometry, so the real phase composition is close to $y = 10/9$. It is supposed that the established data will also be characteristic of transition metal oxide nanocrystals within a homogeneity range. The acquired results are of general interest and can be used in vacancy ordering studies of highly nonstoichiometric nanocrystals.

This study was carried out within the framework of State Assignment to the Institute of Solid State Chemistry of the Ural Branch of the Russian Academy of Sciences (assignment no. 0397-2019-0001) and supported by the Russian Foundation for Basic Research (grant no. 19-03-00051a). The preparation of $TiO_{10/9}$ phase was supported by the Russian Science Foundation (grant no. 14-23-00025). The electronic structure calculations were performed on the Uran supercomputer at the N. N. Krasovskii Institute of Mathematics and Mechanics of the Ural Branch of the Russian Academy of Sciences. The authors are grateful to E. Yu. Gerasimov (G. K. Boreskov Institute of Catalysis, Siberian Branch of the Russian Academy of Sciences) for carrying out the HRTEM experiments.

References

1 E. Hilti, *Naturwissenschaften*, 1968, **55**, 130.
2 E. Hilti and F. Laves, *Naturwissenschaften*, 1968, **55**, 131.
3 D. Watanabe, J. R. Castles, A. Jostsons and A. S. Malin, *Nature*, 1966, **210**, 934.
4 D. Watanabe, J. R. Castles, A. Jostsons and A. S. Malin, *Acta Crystallogr.*, 1967, **23**, 307.
5 D. Watanabe, O. Terasaki, A. Jostsons and J. R. Castles, in *The Chemistry of Extended Defects in Non-Metallic Solids*, eds. L. Eyring and M. O'Keeffe, North-Holland, Amsterdam, 1970, pp. 238–258.
6 A. A. Rempel and A. A. Valeeva, *Mendeleev Commun.*, 2010, **20**, 101.
7 A. A.Valeeva, A. A. Rempel and A. I. Gusev, *JETP Lett.*, 2000, **71**, 460 (*Pis'ma ZhETF*, 2000, **71**, 675).
8 A. A. Valeeva, A. A. Rempel, W. Sprengel and H.-E. Schaefer, *Phys. Solid State*, 2009, **51**, 924 (*Fiz. Tverd. Tela*, 2009, **51**, 876).
9 A. A. Valeeva, G. Tang, A. I. Gusev and A. A. Rempel, *JETP Lett.*, 2003, **77**, 25 (*Pis'ma ZhETF*, 2003, **77**, 28).
10 A. A. Valeeva, G. Tang, A. I. Gusev and A. A. Rempel, *Phys. Solid State*, 2003, **45**, 87 (*Fiz. Tverd. Tela*, 2003, **45**, 84).
11 A. A. Valeeva and A. I. Gusev, *Phys. Solid State*, 2006, **48**, 1689 (*Fiz. Tverd. Tela*, 2006, **48**, 1598).
12 A. I. Gusev and A. A. Valeeva, *JETP Lett.*, 2012, **96**, 364 (*Pis'ma ZhETF*, 2012, **96**, 400).
13 A. I. Gusev, *JETP*, 2013, **117**, 293 (*ZhETF*, 2013, **144**, 340).
14 A. I. Gusev, *J. Solid State Chem.*, 2013, **199**, 181.
15 A. I. Gusev, *JETP*, 2015, **120**, 851 (*ZhETF*, 2015, **147**, 984).
16 M. G. Kostenko and A. A. Rempel, *JETP Lett.*, 2017, **106**, 157 (*Pis'ma ZhETF*, 2017, **106**, 151).
17 M. G. Kostenko and A. A. Rempel, *JETP*, 2017, **125**, 235 (*ZhETF*, 2017, **152**, 280).
18 M. G. Kostenko and A. A. Rempel, *J. Solid State Chem.*, 2017, **253**, 139.
19 M. G. Kostenko, S. V. Sharf and A. A. Rempel, *Mendeleev Commun.*, 2017, **27**, 251.
20 M. G. Kostenko and A. A. Rempel, *Mendeleev Commun.*, 2018, **28**, 36.
21 D. Watanabe and O. Terasaki, *J. Phys. Soc. Jpn.*, 1968, **25**, 292.
22 A. I. Gusev, *JETP Lett.*, 2001, **74**, 91 (*Pis'ma ZhETF*, 2001, **74**, 96).
23 A. A. Valeeva, K. A. Petrovykh, H. Schroettner and A. A. Rempel, *Inorg. Mater.*, 2015, **51**, 1132 (*Neorg. Mater.*, 2015, **51**, 1221).
24 A. A. Valeeva, S. Z. Nazarova and A. A. Rempel, *Phys. Solid State*, 2016, **58**, 771 (*Fiz. Tverd. Tela*, 2016, **58**, 747).
25 A. I. Gusev, A. S. Kurlov and A. A. Rempel, *JETP Lett.*, 2015, **101**, 533 (*Pis'ma ZhETF*, 2015, **101**, 589).
26 W. Kohn and L. J. Sham, *Phys. Rev.*, 1965, **140**, A1133.
27 R. O. Jones and O. Gunnarsson, *Rev. Mod. Phys.*, 1989, **61**, 689.
28 P. Giannozzi, S. Baroni, N. Bonini, M. Calandra, R. Car, C. Cavazzoni, D. Ceresoli, G. L. Chiarotti, M. Cococcioni, I. Dabo, A. Dal Corso, S. de Gironcoli, S. Fabris, G. Fratesi, R. Gebauer, U. Gerstmann, C. Gougoussis, A. Kokalj, M. Lazzeri, L. Martin-Samos, N. Marzari, F. Mauri, R. Mazzarello, S. Paolini, A. Pasquarello, L. Paulatto, C. Sbraccia, S. Scandolo, G. Sclauzero, A. P. Seitsonen, A. Smogunov, P. Umari and R. M. Wentzcovitch, *J. Phys.: Condens. Matter*, 2009, **21**, 395502.
29 J. P. Perdew, K. Burke and M. Ernzerhof, *Phys. Rev. Lett.*, 1996, **77**, 3865.
30 M. C. Payne, M. P. Teter, D. C. Allan, T. A. Arias and J. D. Joannopoulos, *Rev. Mod. Phys.*, 1992, **64**, 1045.
31 D. A. Andersson, P. A. Korzhavyi and B. Johansson, *Phys. Rev. B*, 2005, **71**, 144101.
32 J. Graciani, A. Márquez and J. F. Sanz, *Phys. Rev. B*, 2005, **72**, 054117.
33 M. G. Kostenko, A. V. Lukoyanov, V. P. Zhukov and A. A. Rempel, *J. Solid State Chem.*, 2013, **204**, 146.
34 M. G. Kostenko, A. A. Rempel, S. V. Sharf and A. V. Lukoyanov, *JETP Lett.*, 2013, **97**, 616 (*Pis'ma ZhETF*, 2013, **97**, 712).
35 M. G. Kostenko, A. A. Rempel, S. V. Sharf and A. V. Lukoyanov, *JETP Lett.*, 2015, **102**, 85 (*Pis'ma ZhETF*, 2015, **102**, 94).

Received: 23rd January 2019; Com. 19/5810